http://ijopaar.com; 2016 Vol. 4(1); pp. 01-07.

Experimental and Computational Analysis of 7-Isopropoxy-3-phenyl-4H-1-benzopyran-4-one

C. N. Dipunadas [a], V. Bena Jothy [a*], I. Hubert Joe [b]

[a]Department of Physics and Research Centre, Women's Christian college, Nagercoil-629 001
[b]Department of Physics and Research Centre, Mar Ivanios College, Nalanchira-695015

Email: benaezhil@yahoo.com
dipunaabynraj@gmail.com

Date of revised paper submission: 07/12/2016; Date of acceptance: 16/12/2016
Date of publication: 29/12/2016; *First Author / Corresponding Author; Paper ID: A16403.
Reviewers: Baqri, S. R., India; Ezeamama, A. E., USA.

Abstract

Non-hormonal isoflavone derivative 7-Isopropoxy-3-phenyl-4H-1-benzopyran-4-one (7I3P4H) is used for prevention and treatment of postmenopausal osteoporosis. It is also used for reducing bone loss caused by chronic kidney diseases and paralysis associated with stroke. Optimized geometry and Natural Bond Orbital (NBO) analysis of 7I3P4HB carried out to demonstrate the various intra-molecular interactions that are responsible for the stabilization of this molecule leading to its medicinal activity. Ultraviolet Absorption (UV) spectra have been recorded and analyzed. Energy gap has been calculated from Frontier Molecular Orbital Analysis with the help of B3LYP/6-311++G (d, p) method.

Keywords: Isoflavonoid, NBO, UV-Vis, HOMO-LUMO.

1. Introduction

7-Isopropoxy-3-phenyl-4H-1-benzopyran-4-one is an important member of the isoflavone family. This synthetic flavonoid is reported to stimulate the activity of osteoblasts, to promote deposition of calcium and the formation of mineralized nodules by newborn rat calvarial osteoblasts-like cells as well as the activity of alkaline phosphatase. It exerts a protective action against parathyroid hormone. [1-3].

2. Experimental Analysis

7I3P4H purchased as powder from Sigma Aldrich with a stated purity of greater than 97% was used without further purification. FT-IR spectra was recorded in the region 400-4000 cm^{-1} with the aid of Perkin Elmer Spectrometer and FT-Raman spectra was recorded in the region 50-4000 cm^{-1} using BRUKER RFS 27 SPECTROMETER using 1064 nm excitation from an Nd: YAG laser source with spectral resolution of ±2 cm^{-1}. UV absorption spectra of the compound were examined in the range 200-400nm based on ASTME 169-04 using Varian, CARY 100 BIO UV-Visible Spectrophotometer in methanol solution. ^{1}H and ^{13}CNMR spectra of 7, 8-DH4PC.H_2O was recorded with the aid of Bruker AVANCE III 500 MHz (AV500) multi nuclei solution NMR Spectrometer. Thermal analytical studies were carried out by using a SDT Q600 V20.9 Build 20 in an inert nitrogen atmosphere.

3. Computational Analysis

Geometry optimizations and vibrational spectral investigations have been performed using Becke-3-Lee-Yang-Parr (B3LYP) gradient correlation functional with the basis set B3LYP/6-

311++G(d,p) using Gaussian'09 program package. NBO calculations were performed using NBO 3.1 program as implemented in the Gaussian'09 package. Considering solvent effect, electronic properties such as HOMO and LUMO energies were determined by DFT approach [4–7]. UV-Vis spectral analysis was performed by theoretical calculation using Gaussian 09 program package. Moreover, changes in the thermodynamic functions (heat capacity, entropy, and enthalpy) were assigned for different temperatures from the vibrational frequency calculations of the title molecule.

4. Results and Discussion:

4.1 Optimized Geometry

Structural analysis of the ground state of 7I3P4H has been performed using B3LYP/6-311++G (d,p) basis set. Optimized structure of 7I3P4H is shown in Fig.1 and optimized structural parameters along with crystallographic bond parameters from CIF file are summarized inTable.1. As bond length depends on the bond order, orbital hybridization and resonance or delocalization of π-electrons of the molecule with various bond parameters have been analysed and assigned. Double bond C_{13}-O_{14} length (1.23Å) is greater than the expected range 1.18-1.21Å owing to the effect of resonance. Entire C-H bond lengths of 7I3P4H averages to 1.08 Å except for methoxy groups, where it averages to 1.09 Å since electronic charge is back-donated from the lone pair oxygen atom to σ* orbital of C-H bonds, followed by the increase in C-H bond distance. C-O bond lengths surrounding O_{26} exhibits high value than the expected region 1.342-1.365Å and bond angles C–C–O and O–C–O generally occurs around 120° gets distorted due to resonance effect of carbon atoms as well as inter electronic interaction effect within the coumarin moiety.

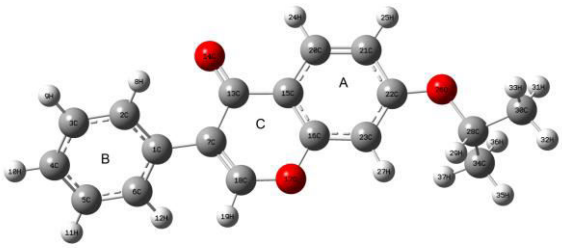

Figure.1. Optimized molecular structure of 7I3P4H

Table.1: Optimized Bond lengths (Å) and Bond Angles (º) of 7I3P4H

Bond Length	Exp (Å)	Theo. (Å)	Bond angle	Exp (º)	Theo. (º)
C_2-H_8	0.930	1.0813	C_7-C_{13}-O_{14}	123.07	123.41
C_3-H_9	0.931	1.0844	O_{14}-C_{13}-C_{15}	122.46	122.31
C_4-H_{10}	0.930	1.0842	C_{15}-C_{16}-O_{17}	121.30	121.14
C_5-H_{11}	0.930	1.0844	O_{17}-C_{16}-C_{23}	115.35	116.05
C_6-H_{12}	0.930	1.0847	C_{16}-O_{17}-C_{18}	118.15	118.82
C_{13}-O_{14}	1.232	1.226	C_{21}-C_{22}-O_{26}	115.00	115.07
C_{16}-O_{17}	1.374	1.3692	C_{23}-C_{22}-O_{26}	125.33	125.07
O_{17}-C_{18}	1.353	1.3531	C_{22}-O_{26}-C_{28}	120.14	121.24
C_{18}-H_{19}	0.930	1.0819	O_{26}-C_{28}- H_{29}	109.87	108.38
C_{20}-H_{24}	0.930	1.0832	O_{26}-C_{28}-C_{30}	105.46	105.67
C_{22}-O_{26}	1.361	1.3545	O_{26}-C_{28}-C_{34}	109.89	110.42
C_{23}-H_{27}	0.930	1.0801	C_7-C_{18}-O_{17}	126.01	125.85
O_{26}-C_{28}	1.443	1.4479			
C_{28}-H_{29}	0.980	1.0955			
C_{30}-H_{31}	0.960	1.0929			
C_{30}-H_{32}	0.959	1.0928			

C_{30}-H_{33}	0.961	1.0916			
C_{34}-H_{35}	0.962	1.0933			
C_{34}-H_{36}	0.961	1.093			
C_{34}-H_{37}	0.961	1.0916			

4.2 Natural Bond Orbital Analysis

NBO analysis has been performed on 7I3P4H at TDDFT/ B3LYP/6-311++G (d,p) level to expound the intramolecular, re-hybridization and delocalization of electron density within the molecule [8]. Resulting stabilization energy E (2) 1.54 Kcal/mol, (Table 2) associated with the hyperconjugative interactions $LP_1O_{26}\rightarrow\sigma^*(C_{28}\text{-}H_{29})$ gives the measure of weak electrostatic C-H…O intra-molecular hydrogen bonding which is very significant in the enrichment of the biological activity of this compound [9-11]. C_{13}-C_{15} is bent by an angle of 2.0° which lies in the strong charge transfer path of O_{14} in ring system having high stabilization energy 28.15 Kcal/mol confirmed from sp hybridized lone pair $LP_2O_{14}\rightarrow\sigma^*C_{13}\text{-}C_{15}$ interactions. An intra-molecular interaction is formed by the orbital overlap between $\sigma O_{17}\text{-}C_{18}$ and $\sigma^*O_{17}\text{-}C_{18}$, results in intramolecular charge transfer causing stabilization of the system thereby elongating corresponding bond lengths (C_{16}-O_{17}=1.37 Å; O_{17}-C_{18}=1.35 Å). Increase in stabilization energy around the methyl groups elongates the corresponding bond lengths.

Table 2. Second order perturbation analysis of Fock matrix using NBO basis.

Donor (i)	ED(i) (e)	Acceptor (j)	ED(j) (e)	E(2)[a] (kJ mol^{-1})	E(j)–E(i)[b] (a.u)	F(i,j)[c] (a.u)
LP_1O_{26}	1.97623	$\sigma^*C_{28}\text{-}H_{29}$	0.01319	1.54	0.93	0.034
LP_2O_{14}	1.88373	$\sigma^*C_{13}\text{-}C_{15}$	0.06424	28.15	0.48	0.105
$\sigma O_{17}\text{-}C_{18}$	1.97765	$\sigma^*O_{17}\text{-}C_{18}$	0.02954	42.98	0.63	0.147
$\sigma C_{34}\text{-}H_{37}$	1.98711	$\sigma^*C_{34}\text{-}H_{35}$	0.00514	56.07	4.97	0.472
$\sigma C_{34}\text{-}H_{37}$	1.98711	$\sigma^*C_{34}\text{-}H_{36}$	0.00813	9.40	2.96	0.149
$\sigma C_{34}\text{-}H_{37}$	1.98711	$\sigma^*C_{34}\text{-}H_{37}$	0.00624	19.88	3.33	0.230

4.3 UV-Vis Analysis

UV absorption spectrum of 7I3P4H recorded in methanol is shown in Fig 2. TDDFT/ B3LYP/6-311++G (d, p) basis set method have been used to determine the low-lying excited states of 7I3P4H. The calculated excitation energies, absorbance and oscillator strength (f) for the title molecule were compared for the solvent methanol with the experimental values and are tabulated in Table 3. HOMO and LUMO orbital take part in chemical stability. In view of calculated absorption spectra, the wavelength 299 nm corresponds to the electronic transition from the HOMO to LUMO with 93% major contribution and only 2% minor contribution is viewed while 255 nm corresponds to electronic transition from HOMO-4 to LUMO with 58% contribution.

Table 3. UV–Vis excitation energy and oscillator strength of 7I3P4H for methanol solvent

No	Wave length(nm)		Energy (eV)	Oscillator Strengths	Major contributes	Minor contributes
	Exp.	Cal.				
Solvent:Methanol						
1		309	4.0	0.0001	H-4->LUMO (11%),	H-2>LUMO(56%)

					H-3->LUMO (29%)	
2	299	299	4.1	0.0383	HOMO->LUMO (93%)	H-1->LUMO (2%)
3		288	4.3	0.1957	H-1->LUMO (88%)	HOMO>L+1(4%)
4		263	4.7	0.2322	H-3->LUMO (41%), H-2->LUMO (22%)	HOMO->L+1(28%) H-2->L+1 (2%)
5		262	4.7	0.4222	H-4->LUMO (14%), H-3->LUMO (11%), H-2->LUMO (17%)	HOMO->L+1 (50%) H-1->LUMO (2%), H-1->L+1 (3%)
6	255	258	4.8	0.0313	H-4->LUMO (5%), H-3->LUMO (11%)	H-1->L+1 (15%) H-1->L+2 (3%), HOMO->L+1(7%)

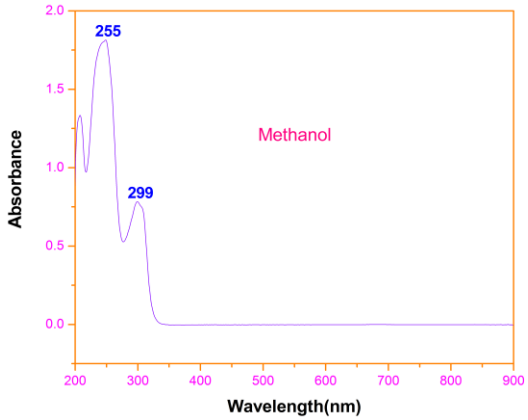

Fig.2. UV-Vis spectra of 7I3P4H

4.4 Frontier Molecular Orbital Energies Analysis

Energies of Highest Occupied Molecular Orbital (HOMO) and the Lowest Unoccupied Molecular Orbital (LUMO) are computed at B3LYP/6-311++G(d,p) level. Substitution in coumarin at various positions perturbs electronic transitions. Molecular orbital plots of the frontier orbitals for the ground state of 7I3P4H molecule (HOMO, LUMO) are shown in Fig.3. In 7I3P4H, HOMO is localized on phenyl ring B with oxygen atom of carbonyl group and ring oxygen atom. LUMO populates on bonded carbon atoms C_{13}-O_{14}, C_{22}-O_{26}, and C_{16}-C_{17}. Energy values of LUMO, HOMO and their energy gap reflect the chemical activity of the molecule. In addition, Lower HOMO-LUMO energy gap shows the possibility of intramolecular charge transfer analysis and confirms the bioactivity of the molecule [14-16]. Optimized electronic energy of 7I3P4H is -955.2426 Hatree. Frontier orbital energy gap (E_{HOMO}–E_{LUMO}) found to be -4.67eV that is a critical parameter in determining electrical transport properties and good antioxidant efficiency. Calculated energy values in gas phase are shown in table.4.

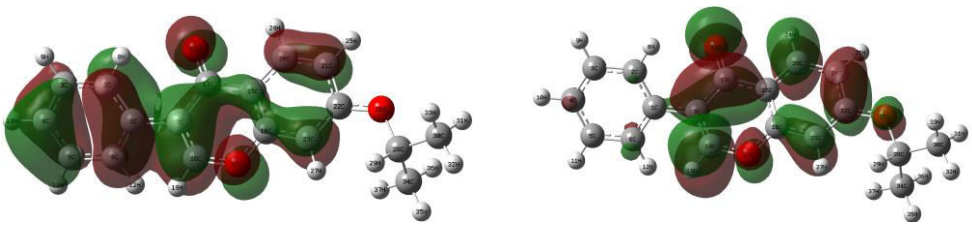

Fig.3 HOMO-LUMO Images of 7I3P4H

Table.4 Calculated energy values of 7I3P4H in gas phase

B3LYP/6-311 G(d,p)	Values
E_{Total} (Hartrees)	
HOMO(eV)	-6.3895086
LUMO(eV)	-1.71214123
Energy Gap (HOMO-LUMO) (eV)	-4.67736737

4.5 NMR Analysis

^{13}C and ^{1}H NMR theoretical and experimental chemical shifts and the assignments of 7I3P4H are presented in Table 5 and values relative to TMS and experimental spectra are shown in Fig. 4(A), (B). Chemical shifts ^{13}C atom double bond with oxygen atom O_{14} having chemical shift 175 ppm is mostly localized on periphery of the molecules as compared to that for other heavier atoms. Overlapped areas of the spectrum of aromatic carbons show signals with chemical shift values from 100 to 150 ppm [12,13]. Phenyl ring carbons without any other substituent assigned around at δ130 ppm. Chemical shift value of C_{22} and C_{16} atoms significantly differs in high shift positions due to the influence of electronegative oxygen atom. Aromatic protons in the region δ 6.0 to 7.9 are indicated by the appearance of a singlet. Chemical shift at 8.2 for H_{24} atom are the highest proton happens due to the intra-molecular charge transfer associated with carbonyl group of chromone moiety. Oxymethine carbon C_{28} shows chemical shift at 70.7 ppm. Side chains C_{28}-C_{34} and C_{28}-C_{30} with methyl group have highest proton H_{37} at 4.7 ppm and H_{32} at 4.6 ppm respectively.

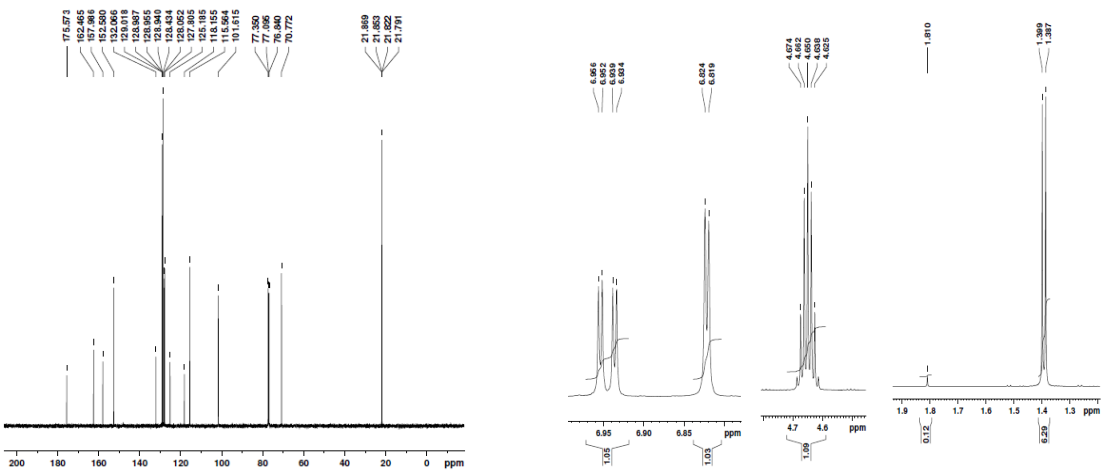

Figure 4 (A) ^{13}C and **4 (B)** ^{1}H NMR Spectra of 7I3P4H

Table 5. Experimental and theoretical ^{13}C and ^{1}H isotropic chemical shifts of 7I3P4H

^{13}C NMR	Theoretical Chemical Shifts	Experimental Chemical Shifts	^{1}H NMR	Theoretical Chemical Shifts	Experimental Chemical Shifts
	$CDCl_3$	$CDCl_3$		$CDCl_3$	$CDCl_3$
C_1	133.4	132.1	H_8	8.2	8.2
C_2	128.5	128.4	H_9	7.7	7.6
C_3	128.9	128.9	H_{10}	7.8	7.6

C_4	128.9	128.9	H_{11}	7.8	7.6
C_5	127.8	127.8	H_{12}	7.6	7.5
C_6	129.4	128.9	H_{19}	8	7.9
C_7	130.4	129.0	H_{24}	8.2	8.2
C_{13}	175.7	175.6	H_{25}	7.2	6.9
C_{15}	125.5	125.2	H_{27}	7.1	6.9
C_{16}	161.5	157.9	H_{29}	4.8	4.7
C_{18}	156.5	152.6	H_{31}	1.7	1.6
C_{20}	128.3	128.1	H_{32}	4.5	4.6
C_{21}	118.7	118.2	H_{33}	1.7	1.8
C_{22}	166.2	162.5	H_{35}	1.4	1.4
C_{23}	99.8	101.6	H_{36}	1.3	1.4
C_{28}	71.4	70.7	H_{37}	4.9	4.7
C_{30}	21.8	40.3			
C_{34}	21.6	21.7			

5. Conclusion

Optimized molecular structure and fundamental vibrational modes of the title compound have been precisely analyzed and assigned. Ring C-O bond lengths have been reduced due to the fusion of benzene ring with the α-pyrone ring. Weak electrostatic C-H…O intra-molecular hydrogen bonding is confirmed by NBO analysis. Electronic transition from the HOMO to LUMO with 93% major contribution corresponds to 299 nm observed in UV-Vis analysis. Intra-molecular charge transfer associated with carbonyl group of chromone moiety has higher chemical shift. Presence of a methyl group as well as the lower HOMO-LUMO energy gap confirms the bioactivity and intramolecular charge transfer analysis of title molecule.

References

1. Polkowski, K. and Aleksander P. Mazurek, 2000, Acta Poloniae Pharmaccutica - drug Research, 57, 135.
2. Vitale, D. C., Cateno Piazza, Barbara Melilli, Filippo Drago, Salvatore Salomone, 2013, Eur J Drug Metab Pharmacokinet 38, 15.
3. Qiang Ren, M., Gerda Kuhn Jochen Wegner, Jie Chen, 2001, European Journal of Nutrition, 40.
4. Petersilka, M., Gossmann, U. J., Gross, E. K. U., 1966, Phys. Rev. Lett. 76, 1212–1215.
5. Bauernschmitt, R., Ahlrichs, R., 1996, Chem. Phys. Lett. 256, 454–464.
6. Jamorski, C., Casida, M. E., Salahub, D. R., 1996, J. Chem. Phys. 104, 5134–5147.
7. Runge, E., Gross, E. K. U., 1984, Phys. Rev. Lett. 52, 997–1000.
8. Sudha S. et al., 2011, Journal of Molecular Structure 985, 148–156.
9. Jeffrey, George. A, 1997, An introduction to hydrogen bonding, Oxford University Press.
10. Marques, M. P. M., Amorim da Costa, A. M., Ribeiro-Claro, P. J. A., 2001, J. Phys. Chem. A 105, 5292–5297.
11. Ribeiro-Claro, P. J. A., M., Drew, G. B. and Felix, V., 2002, Chem. Phy. Lett. 356, 318–325.
12. Kalinowski, H. O., Berger, S. and Braun, S. 1988, Carbon-13 NMR Spectroscopy, John Wiley & Sons, Chichester.
13. Pihlaja, K., Kleinpeter, E. (Eds.), 1994, Carbon-13 Chemical Shifts in Structural and Sterochemical Analysis, VCH Publishers, Deerfield Beach.

14. Kurt, M., Chinna Babu, P., Sundaraganesan, N., Cinar, M. and Karabacak, M., 2011, Spectrochim. Acta Part A 79, 1162–1170.

15. Padmaja, L., Ravikumar, C., Sajan, D., Joe, I. H., Jayakumar, V. S., Pettit, G. R. and Nielsen, O. F., 2009, J. Raman Spectrosc 40, 419–428.

16. Ravikumar, C., Joe, I. H. and Jayakumar, V. S., 2008, Chem. Phys. Lett. 460, 552–558.